Check for updates

Stretchable reflective coating for soft optical waveguides and sensors†

Simone Lantean, ‡*[a] Matteo Lo Preti ‡[ab] and Lucia Beccai *[a]

Soft robots must embody mechanosensing capabilities to merge with and act in the environment. Stretchable waveguides are making a mark in soft mechanical sensing since they are built from pristine elastomers. Therefore, they are insensitive to electromagnetic fields and weakly affect the deformations of the robot. However, issues in light-shielding, signal decoupling, and core-cladding interfaces are still open challenges. In this work, titanium oxide particles (TiO_2) are dispersed in silicone elastomers to develop a soft optical shield coating. Results show that the added particles do not harden the matrix and reduce light transmission. Almost full NIR shielding is achieved by adding 1.0 vol% of TiO_2 in 150 μm thick films. These properties make the proposed shielding coating an excellent candidate for soft mechanosensing. An open-access tool is developed to design soft optical devices by programming light transmittance at desired wavelengths by tuning, both, TiO_2 concentration and film thickness. Finally, two proof-of-concepts are demonstrated, a soft waveguide and a soft strain sensor, by integrating the developed material to shield a transparent PDMS resin and a semi-transparent Ecoflex00-10 matrix, respectively. The soft waveguide can stretch up to 40% with very low optical loss, while the optical strain sensor can detect strain up to 90%. In both cases, bending, folding, and indentation of the devices have a significantly low impact on light transmission. These results can pave the way to design new optical transmission devices and sensors that exploit light reflection and that allow for discriminating different types of mechanical stimuli in soft robots.

Introduction

Mechanosensing is fundamental in robotic systems as it allows adaptation and reaction to unexpected situations. On one hand, sensing external mechanical cues (*e.g.*, pressure, directional forces, vibration, *etc.*) allows exploring the outer world and manipulating unknown objects. On the other hand, robots need to reconstruct their own movements to be controlled.[1] This is critical in soft robots as they need to discriminate various mechanical stimuli. The sensors must be highly compliant not to physically burden the robot body due to the application of thick and stiff artificial skins on its surface. Also, in the case of distributed sensing, high wiring volumes should be avoided by developing *ad hoc* transduction principles.

In this vision, stretchable waveguide sensors are gaining increased attention because of some peculiar aspects,[2,3] among which are their insensitivity to electromagnetic fields and

intrinsic safety. Moreover, the optically clear soft matrix is in direct contact with the environment, protecting the electronic components underneath.[4] This hugely increases the robustness and lifespan of these kinds of sensors. Yet, there is still a need to avoid signal dispersion and losses from the transduction medium effectively and to decouple possible sources of light variations.

In general, optical waveguides are composed of two elements: (i) a high refractive index optical medium (the core) and (ii) a low refractive index material (cladding) surrounding the core. This design allows light to be confined within the core by internal light reflection and avoiding optical loss upon bending of the waveguide.

When using this design in soft robotics, the applied materials, besides optical properties, must fulfill specific mechanical requirements. Indeed, the material must be highly deformable and stretchable, *i.e.*, low elastic modulus and high elongation at break, to enhance the compliance of the final device.[5]

Conventional optical transducers and waveguides (*i.e.*, fibers) are made of silica glass. They are rigid, stiff, and fragile, thus, not suitable for developing soft sensors, or for being integrated in soft actuators or soft robot bodies in general. In the past, much effort was put into replacing traditional glass-based optical fibers with polymeric materials such as

[a] *Soft BioRobotics Perception, Istituto Italiano di Tecnologia (IIT), Genova, Italy.*
 E-mail: simone.lantean@iit.it

[b] *The BioRobotics Institute, Scuola Superiore Sant'Anna, Pontedera, Italy*

‡ These authors contributed equally.

polymethylmethacrylate[6] (PMMA), cyclic olefin copolymers,[7] and hydrogels.[8] However, the reduced compliance and stretchability of these materials limited their application in more demanding applications. Recently, silicones and polyurethane elastomers have emerged as good candidates for soft optical devices as they combine low elastic moduli (in general lower than 5 MPa) and a high elongation at break (>300%), with low optical absorbance in the visible (VIS) and near infra-red (NIR) range.[3] In the literature, several examples of soft and stretchable optical devices working in the NIR range can be found based on the conventional core-cladding, or only core, designs.[9,10]

In the last decade, there has been increasing research effort to develop soft waveguides, *i.e.*, deformable light conductors. Martincek *et al.* developed a new fabrication method to produce stretchable light fibers made of polydimethylsiloxane (PDMS) elastomers with enhanced control in their length and diameter, without a cladding material.[11] Massinne and coauthors fabricated silicone-based waveguides by coupling different silicone elastomers as core and cladding materials (Nusil LS-6941 and Dow Corning Sylgard 184, respectively). The optical waveguides were able to withstand stretching up to 30% with relatively low optical loss, and they were tolerant to bending up to curvature radii larger than 7 mm.[12] Guo *et al.* recently developed stretchable PDMS-based waveguides, where the refractive index between the core and the cladding was tuned by modifying the ratio between the resin and the cross-linkers. Embedding thermal-sensitive upconversion nanoparticles in the core, the authors developed a temperature-sensitive optical fiber stretchable up to 80%.[13]

In parallel, new designs of stretchable optical sensors were introduced. Harnett *et al.* used polyurethanes and silicones, as core and cladding, respectively, in optical fibers capable of detecting strains up to 100%;[14] conversely, Zhao *et al.* used silicone for the core and polyurethane for the cladding in a tactile sensor demonstrated in a prosthetic hand.[15] Similar stretchable optical fibers based on silicone gels were doped with thermochromic pigments to develop haptic sensors sensitive to thermal variations.[16] H. Bai *et al.* decoupled bending, stretching and localized pressure in stretchable fibers by embedding a discrete color-block pattern. The variations of light intensity and chromaticity were read simultaneously by coupling two polyurethane cores and a silicone cladding.[17] Moreover, Leber *et al.* showed an optical sensor capable of measuring strain up to 300% by fabricating fibers with a polystyrene core and a fluorinated polymer cladding.[18] Also, J. Guo and coauthors developed a 1 cm-long optical strain sensor by adding dyes in a PDMS fiber. The fabricated sensors could detect strains up to 100% and be tolerant to bending at curvature radii larger than 6 cm.[19] Recently, Heiden *et al.* 3D printed biodegradable stretchable waveguides based on a gelatin-based hydrogel.[20]

Despite the excellent results in terms of stretchability of the components, several issues must still be addressed both for waveguides used as connecting optical components and as strain sensors. Indeed, their reliability from the mechanical point of view, but also for the optical signal transmission and sensing output, is strongly limited by the aspects described in the following:

(i) Debonding at the core and cladding interface. The combination of two elastomers having a different chemical nature, *e.g.*, polyurethane-silicone and polystyrene-fluorinated polymers, is not trivial as their interfacing may lead to unpredicted optical effects and early rupture of the component. Debonding at the interface may occur upon repeated high stretching loads and several mechanical deformations,[18] generating defects and voids and thus altering light transmission within the core material.

(ii) Environmental light-shielding. As the developed devices are commonly not shielded, environmental light, as well as objects made of materials with a different refractive index, may interfere with light transmission in the optical devices.

(iii) Concurrent mechanical stimuli. Soft optical sensors are very sensitive to stretching, compression, bending, and twisting, and all such mechanical stimuli contribute to the variation of the optical signal. Hence, the sensors must be designed to detect only the desired stimulus.

(iv) Safety and hazardous risks. Mechanical sensors are often produced starting from castable polyurethanes containing isocyanates, which are harmful to human health. Thus, safety protocols are applied during the fabrication process, potentially limiting their large-scale production.

In this work, all the above aspects are addressed by using silicone-based matrices only, thus avoiding safety issues. A coating layer capable of shielding the external light is developed, allowing selectivity and improving the adhesion between the core and the cladding materials. Moreover, the reflective coating is used to build a soft strain sensor that is not affected by bending, folding, and indentation.

A good strategy to avoid debonding at the interface between the core and the cladding would be to apply the same elastomeric matrix for both parts of the waveguide. However, using the same material prevents internal reflection and light guiding since the refractive indices between the core and cladding cannot have large variations. Our strategy involves developing a new highly reflecting and deformable coating with the two-fold function of the cladding and shielding materials in optical waveguides. This is achieved by adding highly reflective particles in elastomeric materials and by exploiting the internal reflection mechanism to guide light within the optical device.

Several compounds can be added to organic matrices to develop reflective coating. This was deeply investigated to produce cool coatings and protections in, *e.g.*, buildings and solar cells.[21–23] A similar approach can be applied to develop efficient soft devices since the optical properties of the fillers are, in principle, independent of the host matrices. In the past, different materials were added to polymeric matrices to enhance the reflective power of the coatings, such as metal particles (Al, Ag, and Cu),[21] metal oxide particles (TiO_2, ZnO, CeO_2, and Y_2O_3),[23–28] and organic pigments.[22]

Among these, TiO_2 particles are the perfect candidate to produce reflective coatings as this filler exhibits superior optical properties. Also, the particles are commercially available.

Thus, no complex synthesis method is required. In particular, rutile is the most thermodynamically stable phase, it exhibits the highest reflectivity to near-infrared (NIR) radiation,[29] and its optical properties are not influenced by either temperature or moisture.[23]

In this work, two different optical devices are proposed, *i.e.*, a waveguide and a strain sensor. PDMS is chosen for the waveguide fabrication as it is thermally stable and isotropic and has nominally zero absorbance in the NIR range.[11] On the other hand, another silicon-based elastomer, Ecoflex00-10, is used as the core material for the strain sensor as it is not fully transparent in the NIR range, and its light absorption can be exploited to evaluate the strain of the material. Micrometric TiO_2 particles (5 μm) are added to PDMS or Ecoflex10 to develop a highly reflective shielding coating for both the waveguide and the strain sensor. By tuning the composite film thickness and the concentration of TiO_2 particles, composite coatings that are able to shield and reflect light without stiffening the material are fabricated. Then, an open-access platform is developed, which determines the TiO_2 concentration and the film thickness needed for a specific light transmittance at a known wavelength, for developing new optical soft devices. Finally, as proof-of-concepts, a PDMS-based waveguide and an Ecoflex-based strain sensor are built by using composite films as coatings, proving their superior performance in terms of selectivity and light-shielding.

Methodology

Sample preparation

Titanium oxide and rutile particles (TiO_2, <10 μm) were purchased from Sigma Aldrich and dispersed in a commercial polydimethylsiloxane resin (Sylgard 184, Dow Corning) in different volume concentrations: 0.10, 0.25, 0.50, and 1.00 vol% with respect to the prepolymer content. The cross-linker was added at the 10:1 ratio to all the prepared formulations. For PDMS-based waveguides, the cross-linker was added at the 20:1 ratio to enhance the deformation of the device.

For the optical sensors, the TiO_2 particles were added at 1.00 vol% to a mixture 1:1 of Ecoflex-0010 part A and Ecoflex-0010 part B (Smooth-on).

The prepared formulations were mixed for 30 seconds in a planetary centrifugal mixer (Thinky ARE-250) and defoamed for 30 seconds to improve the particle dispersion and homogenize the formulations. After, the formulations were carefully degassed in a vacuum chamber for about 10 minutes to eliminate air bubbles in the resin. Once cast, the formulations were again placed in a vacuum chamber for 10 minutes. Curing was performed in an oven (Vacutherm, Thermo Scientific) at 60 °C and lasted 6 hours for PDMS and 2 hours for Ecoflex-based samples.

All the molds used in this work were fabricated *via* a Fused Filament Fabrication (FFF) 3D printer (Ultimaker S3) by extruding acrylonitrile butadiene styrene (ABS) filaments.

The photoemitters (PEs) used in the devices (infrared LEDs, VSMY1850) have a peak of emission at 850 nm, matched to the peak of reception of the photoreceivers (PRs) (silicon NPN epitaxial planar detectors, VEMT2023SLX01).

Characterization

Optical images were taken using a HIROX KH-8700 digital optical microscope at different magnifications.

Fourier-transform Infrared spectroscopy (FTIR) in ttenuated total reflection (ATR) mode was performed by (Shimadzu, Miracle 10) monitoring the peak centered at 2160 cm^{-1} corresponding to the reacting Si–H groups of the polymeric matrix. All the spectra were normalized to the univariant peak of C–H groups placed at 789 cm^{-1}.

Ultra-violet-visible-near infrared (UV-Vis-NIR) spectrometry was performed by LAMBDA 650 (PerkinElmer), measuring the transmitted light percentage (%T) in the 1100–300 nm range.

Reflectance was measured using a Varian Cary 5000 spectrophotometer equipped with an integrating sphere (Diffuse Reflectance Accessory, Agilent).

The mechanical tensile tests on the composite materials were performed with a ProLine (ZwickRoell) equipped with a 10 N load cell. The samples were cast in a dog bone shape (cross section of 4 × 3 mm, length of 30 mm), preloaded at 0.1 N, and tested with a strain rate of 2 mm s^{-1}.

The soft optical devices were characterized using *ad hoc* tensile test apparatus. The samples were arranged in the setup undergoing an aluminum clamping mechanism. A tensile force was applied by a micrometric servo-controlled translation stage (M-414.1DG, Physik Instrumente, Karlsruhe, Germany) and measured through a uniaxial load cell (Burster 8431 with USB interface 9206, Burster gmbh & co kg, Gernsbach, Germany). The response of the photoreceiver was captured using a DAQ system (USB-6218, National Instruments, Austin, TX, USA). The protocol for the acquisition consisted of: (i) manual adjustment of the distance between the clamps,; (ii) positioning of the sample, (iii) setting the sample in tension, and (iv) selecting the test parameters (*e.g.*, number of cycles, displacement, speed). Each test was performed for 5 cycles up to a displacement of 100% and a speed of 0.5 mm s^{-1}.

Indentation tests were carried out using a second experimental setup. The sample was fixed using a bi-adhesive tape to a Lab Jack (Newport 271, MKS Instruments, Inc.), which was positioned under a force platform. The latter consisted of one orthogonal manual micrometric translation stage (M-105.10, Physik Instrumente, Karlsruhe, Germany) coupled with a micrometric servo-controlled translation stage (M-111.1DG, Physik Instrumente, Karlsruhe, Germany) (for a precision vertical positioning). A Delrin probe was mechanically interfaced to the previous translation stage and to a triaxial load cell (ATI Nano 17, ATI Industrial Automation, Inc., Apex, NC, USA). The probe exerted a vertical force on the sample beneath it. The response of the photoreceiver is captured using a DAQ system (USB-6218, National Instruments, Austin, TX, USA). Each acquisition starts by bringing the stage to the highest vertical position, while the hardware peripherals are initialized. The vertical position is controlled *via* software, such that each acquisition starts at the

same probe–sample distance. The tests were performed for 5 cycles and 30% of indentation depth.

Results and discussion

Formulation characterization

Four different concentrations of TiO_2 particles in PDMS were tested: 0.1, 0.25, 0.5, and 1 vol%. Adding inorganic and more dense fillers (PDMS = 0.98 g cm^{-3} and TiO_2 = 3.5 g cm^{-3}) may lead to the aggregation and sedimentation of the particles causing instability and deterioration of the final properties of the material. The stability of the PDMS–TiO_2 formulations was evaluated on the system at the highest TiO_2 concentration (1 vol%, PDMS_1TiO$_2$) as it is more likely to undergo precipitation and sedimentation. The tested formulation remained stable for more than 6 hours, which is comparable to the curing time of the PDMS (Fig. S1, ESI†). Hence, the investigated system is suitable for conventional casting manufacturing methods.

The effect of TiO_2 particles on the polymerization process of the hosting silicone matrix was investigated. Fourier-transform Infrared (FT-IR) spectroscopy in the attenuated total reflection (ATR) method was used to analyze the infrared spectra of uncured PDMS and cured samples at increasing TiO_2 concentrations. Sylgard 184 cures *via* a platinum-catalyzed hydrosilation reaction between the vinyl groups in the prepolymer and the silane groups (SiH$_4$) contained in the curing agent. Therefore, the polymerization

of the elastomer was monitored following the variation of the peak placed at 2160 cm^{-1}, which is ascribable to the stretching vibration of SI–H groups of the curing agent.[30–32] All the spectra were normalized with respect to the peak placed at 789 cm^{-1}, corresponding to the bending of C–H groups, which are not involved in the polymerization of silicones. The peak related to Si–H groups completely flattened for all the cured samples regardless of the particle concentration (Fig. 1a), demonstrating full curing of the composite materials. This proved that TiO_2 particles do not alter the thermal curing of the PDMS matrix, since the full conversion of the reacting groups was achieved for all the tested samples.

The lowest and the highest TiO_2-loaded formulations (PDMS_0.25TiO$_2$ and PDMS_1TiO$_2$ samples, respectively) were coated on a microscope slide with 150 µm thickness and characterized by optical microscopy to evaluate the dispersion of the fillers in the hosting matrix. The images taken at low magnification (Fig. 1b and c) are of difficult interpretation due to a strong reflection of the microscope light. However, this is a qualitative indication of the reflective properties of the composite films. Images at higher magnification (insets in Fig. 1) showed that TiO_2 particles are well dispersed in the host matrix, indicating that the optical and mechanical properties of the designed coatings were likely to be homogenous.

Optical properties

Ultra-violet-visible-near infrared (UV-Vis-NIR) spectroscopy was used to investigate the optical properties and the shielding
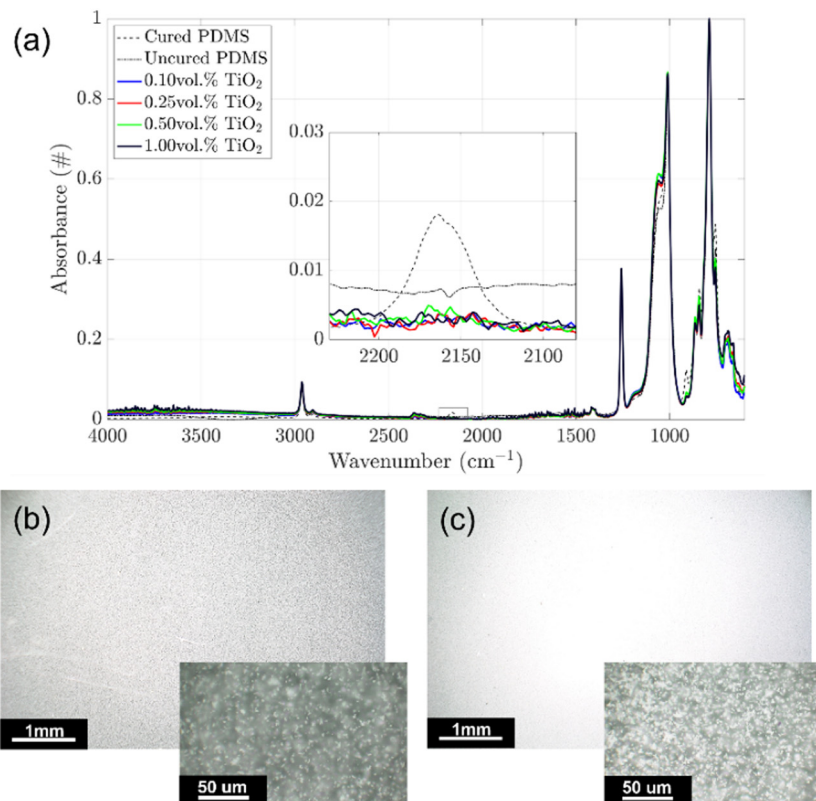

Fig. 1 (a) FT-IR ATR spectra focused on the Si–H reacting groups (2160 cm^{-1}) at increasing TiO_2 particle concentrations (0, 0.1, 0.25, 0.5, and 1 vol%). Optical microscopy images taken at increasing magnifications of PDMS with 0.25 (b) and 1 (c) vol% TiO_2.

capability of the silicone–titania-based samples. Four samples at increasing TiO_2 concentrations (0.1, 0.25, 0.5, and 1 vol%) were coated on a microscope slide with different film thicknesses (50, 75, 150, and 200 μm) and cured in an oven (60 °C, 6 h). Pristine PDMS samples were tested and used as a reference. This characterization can only evaluate a decrease in light intensity (or light transmittance) through the samples. However, since TiO_2 particles are found to be completely reflective,[33] light signal losses must be ascribed to reflecting and scattering phenomena rather than light absorption.[33]

The pure PDMS samples showed 100% light transmittance (zero loss) in the light range from 300 to 1100 nm regardless of the film thickness, proving the well-known transparency in the visible and NIR spectrum of this material (grey dashed line in Fig. 2).[34–36] When TiO_2 particles were added, an overall decrease in light transmittance (%T) was observed. The amount of the optical loss depends on the amount of TiO_2 particles and the film thickness. For instance, the %T values of PDMS_1.0TiO_2 are generally 3 folds lower than those measured for the PDMS_0.1TiO_2 sample (30% vs. 90% in the case of 50 μm thick films). On the other hand, the impact of film thickness seems lower than the concentration of TiO_2 particles, and its influence is lower in the thicker samples (150 μm and 200 μm samples). In general, the lowest values of %T were obtained in the NIR region of the spectrum (800–1100 nm). In particular, almost full NIR shielding (0%T) was achieved for 150 μm- and 200 μm-thick PDMS_1.0TiO_2 samples.

The NIR photoemitters used in the fabrication of the optical devices have an emission spectrum centered at 850 nm of the electromagnetic spectrum. Therefore, the effect of TiO_2 particles concentration and film thickness at this wavelength was evaluated. Fig. 3a shows that for the same layer thickness, the transmittance decreased with the TiO_2 load following a decaying exponential law. Moreover, any significant difference was observed between 150 μm- and 200 μm-thick samples, suggesting the existence of a threshold above which the effect of film thickness is negligible. Fig. 3b underlines the role of the film thickness, and after a fast decay in light transmittance occurring up to 75 μm, the curves flattened, reaching a pseudo-plateau at 150 μm. The effect of the particles' concentration and the film thickness can be combined in order to produce a 3D diagram that describes the variation in light transmittance by varying these two parameters (Fig. 3c).

Based on our experimental data and results, we relied on the universal approximation theorem[37,38] to determine the required vol% of TiO_2 particles to be dispersed in a PDMS matrix to obtain desired transmittance in a layer with a chosen width at a desired wavelength. The resulting graphical user interface is available at the following link (**https://www.math works.com/matlabcentral/fileexchange/114280-tio2-particle-concentration**), and it can be a helpful tool in designing new optical devices by material selection. All the technical details are reported in the ESI.†

To further validate the TiO_2-composite films as reflecting shielding materials, the reflectance of 1 mm thick PDMS_0.1TiO_2
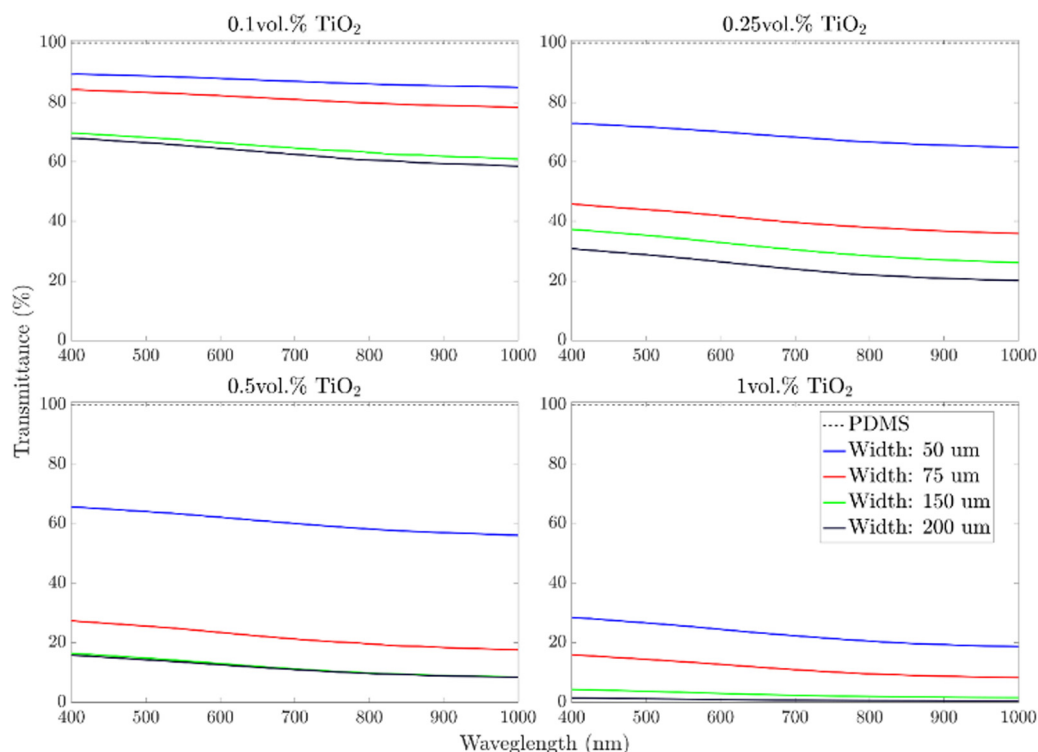

Fig. 2   UV-Vis-NIR spectrometry for 50 μm, 75 μm, 150 μm, and 200 μm thick films of PDMS_0.1TiO_2, PDMS_0.25TiO_2, PDMS_0.5TiO_2, PDMS_1.0TiO_2 samples. The grey dashed line is relative to the reference sample of pristine PDMS.

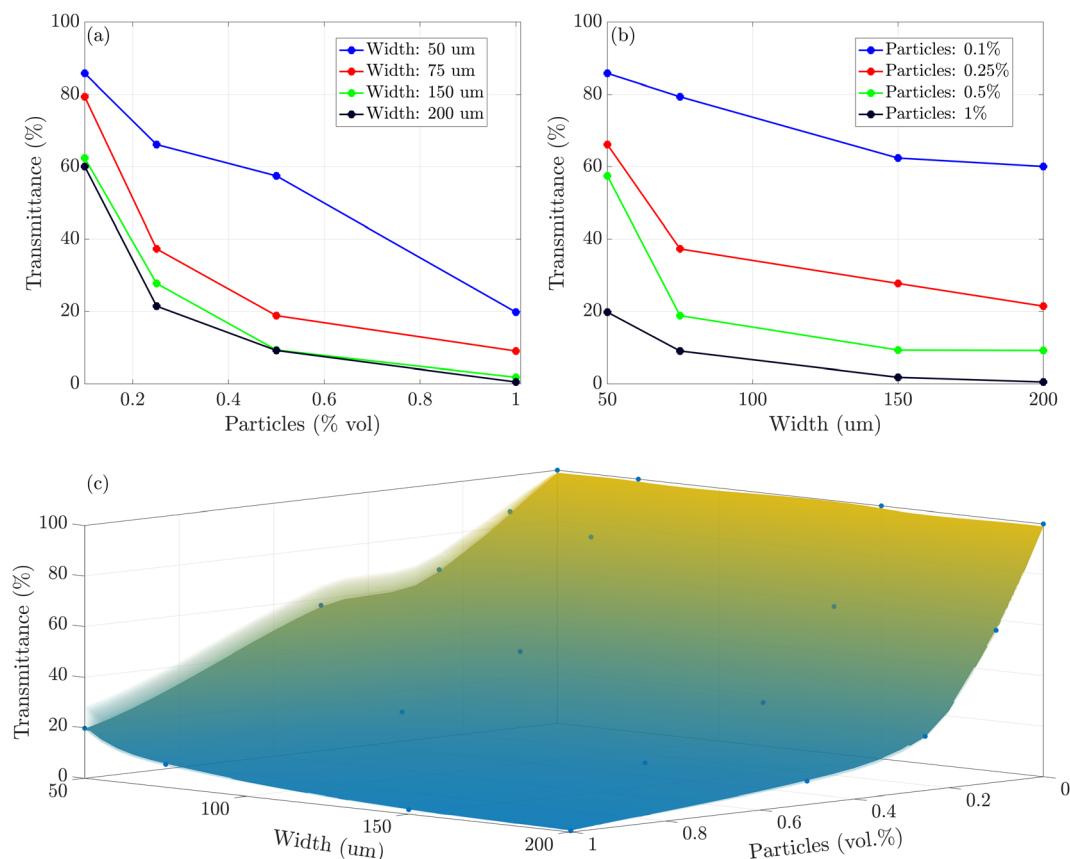**Fig. 3** (a) Effect of the TiO$_2$ concentration in the NIR transmittance for constant film thickness. (b) Effect of the film thickness on the NIR transmission for constant TiO$_2$ concentrations. (c) Combination of the TiO$_2$ concentration and the film thickness on the light transmission. All the graphs refer to 850 nm wavelength.

and PDMS_1.0TiO$_2$ samples was measured (Fig. S2, ESI†). Focusing on the wavelength of the emission spectrum of the optical component (850 nm), the reflectance increased from 70% for the sample with 0.1 vol% of particles to 87% for the sample with the highest load of fillers (*i.e.* 1 vol%). These results confirm the possibility of applying PDMS–TiO$_2$ composite materials as NIR shielding and reflective coatings for optical applications. It is important to mention that the results achieved in terms of light-shielding are only ascribable to the addition of TiO$_2$ particles. Therefore, similar results can be achieved by loading TiO$_2$ particles to different polymeric matrices widening the range of application of the proposed approach.

Mechanical properties

In general, the addition of inorganic particles within a polymeric matrix leads to a stiffening of the final composite material. This limits the deformability of active soft structures and devices and is one of the bottlenecks in developing soft transducers. The stiffening often leads to an increase of the elastic modulus and a decrease in the elongation at break. Both these aspects must be avoided in the fabrication of waveguides and strain sensors, as they limit the compliance of the devices. Indeed, stiffer devices deform under higher forces and have a lower stretching range, *i.e.* the device undergoes rupture at lower elongations.

The mechanical properties of the composite coating were investigated with the aid of uniaxial tensile tests (Fig. S3, ESI†). In Fig. 4, the trends of the elastic moduli at different strains for different concentrations of TiO$_2$ particles are shown. Unlike the expected, all the samples loaded with TiO$_2$ particles showed lower elastic moduli than the pristine PDMS samples. In particular, the samples with the highest concentration of particles (and best shielding properties) have an elastic modulus ~20% lower than net PDMS (1.23 *vs.* 1.46 MPa@5% strain, and 1.13 *vs.* 1.37 MPa@10% strain). However, a clear trend between the concentration of particles and the elastic moduli of the resulting composite materials is not observed.

The silicone matrix's reduction of the elastic moduli by adding TiO$_2$ particles (in rutile and anatase phases) is already reported in the literature.[33,39–41] However, an exhaustive explanation of this trend still does not exist. As no large aggregates were observed by optical microscopy (Fig. 1), the reduction of the elastic moduli cannot be ascribed to defects produced by the addition of TiO$_2$ particles. Most likely, the effect of TiO$_2$ particles is the result of two competing mechanisms: the softening effect of TiO$_2$ particles due to interference with the cross-linking process of the elastomeric matrix (majoritarian effect) and the hardening effect due to the high intrinsic modulus of TiO$_2$ particles (minority effect).[39] However,
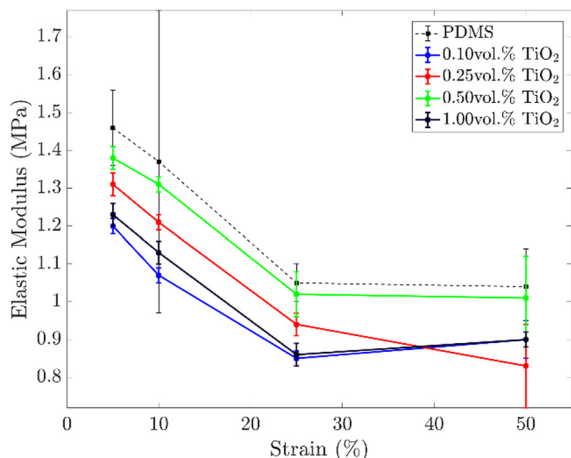
Fig. 4 Elastic module *versus* strain percentage of dog bone PDMS-based specimens at increasing TiO$_2$ particle concentrations. Data are acquired by uniaxial testing.

ATR analysis witnessed that TiO$_2$ particles did not alter the polymerization yield of the silicone matrix, but the full conversion of the Si–H groups was always achieved (see Fig. 1a). Thus, most probably the softening effect is due to a reduction of the cross-linking density of the polymeric network caused by the presence of the inorganic fillers.

The mechanical tests demonstrate that the addition of TiO$_2$ in PDMS does not stiffen the material but results in a softer composite material. Therefore, PDMS–TiO$_2$ composites are good candidates for soft optical devices as they guarantee superior light-shielding properties without affecting the compliance of the waveguides or strain sensors.

Proof-of-concepts: transparent waveguide and strain sensor

As proof-of-concepts, a transparent waveguide and a strain sensor were fabricated *via* a multi-step casting procedure. Regarding the reflective cladding material, UV-Vis-NIR spectroscopy proved that PDMS_1.0TiO$_2$ 200 μm-thick films were already effective in reflecting light in the NIR range. However, to facilitate the casting procedures and improve the tolerance to failure, the thickness was increased up to 1.25 mm. The increase of the cladding thickness is not expected to strongly harden the device as the composite material is softer than the pristine silicone (core material).

The transparent PDMS waveguides were fabricated using a circular and rectangular cross-section and coated/uncoated. In principle, both shapes could be used in the future as optical connectors in soft robotics, and the aim was to evaluate the effect of the shape and the reflecting TiO$_2$ material on the performance of the devices. To improve the deformability of the objects, PDMS 20 : 1 was used as the core material. The strain sensor was designed using a rectangular cross-section, as this shape could in the future allow for the development of extended artificial skins.

Starting from the circular waveguide (Fig. 5a), the fabrication process consisted of the following steps: (i) half of the core
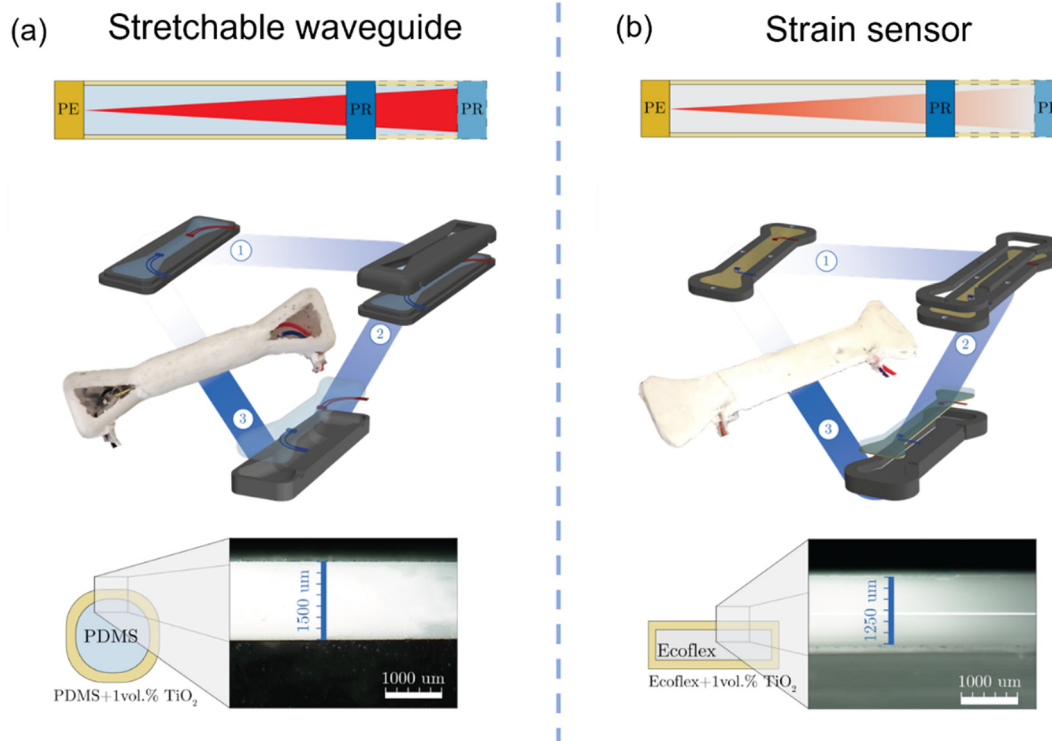

Fig. 5 (a) Circular waveguide, and (b) rectangular strain sensor: top, sketch of the working principles of each device. Middle, Sketch of the fabrication process and picture of the resulting device. Bottom, Optical microscope images taken at the interface between the core and the cladding to evaluate the uniformity and the thickness of the coating. Scale bar is 1 mm.

of the waveguide was poured into a mold, and after curing, the photoemitter and the photoreceiver were glued on the top with Sil-Poxy 30 mm apart; (ii) the top part of the core mold was placed on top of the first one, and PDMS was poured to finally obtain the whole core of the waveguide; (iii) in order to coat the core with the TiO_2 composite, a third mold was used. The coating mold had a rounded cavity in the central body to allow uniform coating on the bottom portion of the waveguide leading to a coating layer of 1.25 mm thickness. After the curing of the first layer, the waveguide was flipped, and the coating process was repeated for the remaining part. Finally, a uniform coating layer of about 1400 μm thickness was obtained at the central rounded section of the waveguide.

In the case of the rectangular strain sensor (Fig. 5b), the fabrication process consisted of the following: (i) the Ecoflex_1.0TiO$_2$ coating was poured into a mold to fabricate the bottom coating and cured. Afterwards, the photoemitter and the photodetector were glued with Sil-Poxy on the bottom layer 20 mm apart; (ii) the core mold was secured on top of the previous one, and pristine Ecoflex-0010 resin was poured to obtain the core of the waveguide; (iii) after curing, the bottom layer and the core were demolded and placed into a third mold to fabricate the coating. The coating mold was 1.25 mm larger in all directions to allow the infiltration of Ecoflex_1.0TiO$_2$ as the lateral and top coating layer. Optical microscopy images showed a uniform coating of 1250 μm thickness. A rectangular PDMS-based waveguide was also produced using the optical components 30 mm apart for comparison with the circular one. A sketch reporting the dimension of the fabricated devices is reported in Fig. S4 (ESI†).

PDMS-based waveguide. Transparent waveguides were characterized with an *ad hoc* tensile testing setup following the variation in the output voltage of the photodetector during the elongation of the device. Stretching the device the optical path is increased, and a variation in light intensity measured by the photoemitter is expected. The relation between the light intensity and the optical path is described by the Lambert–Beer law (eqn (1)):

$$T = I_1/I_0 = e^{-K_\lambda l} \qquad (1)$$

where T is the transmittance, and it is the ratio between the residual light intensity (I_1) and the initial light intensity (I_0). K_λ is the attenuation coefficient of the material at the specific wavelength (λ), and l is the optical path, *i.e.* sample thickness. As K_λ is constant and an intrinsic property of the material, the light transmission scales exponentially with the optical path. However, PDMS is considered transparent in the visible and NIR range of the electromagnetic spectrum (see Fig. 2), therefore, K_λ approaches 0. As K_λ is in the argument of the exponent, T always approaches 1 regardless of the optical path (*i.e.*, the elongation of the waveguide) (eqn (2)).

$$k_\lambda = 0, \quad T = I_1/I_0 = e^{(0 \cdot l)} = 1 \rightarrow I_1 = I_0 \qquad (2)$$

Since the attenuation of the optical signal due to the PDMS material is not zero, a small decay in light transmission was expected.

Fig. 6a shows the voltage variation of the photoreceiver when circular and rectangular, coated, and uncoated waveguides were stretched (5 cycles, 1 mm s^{-1} strain rate). The voltage read by the photoreceiver ranged from 0 V (full light) to 4.8 V (no light). The uncoated rectangular waveguide showed the poorest performance in guiding light as around 25% of strain an abrupt increase in the voltage was observed probably due to border effects. The corresponding rectangular coated waveguide showed improved performance. Yet, an increase in the optical loss was still detected at around 32% of strain. The circular waveguides had the lowest optical losses with very low variation in the optical signal up to 40% of strain. In both cases, the coated devices displayed superior performance proving the efficacy of the reflecting coatings. As rectangular waveguides
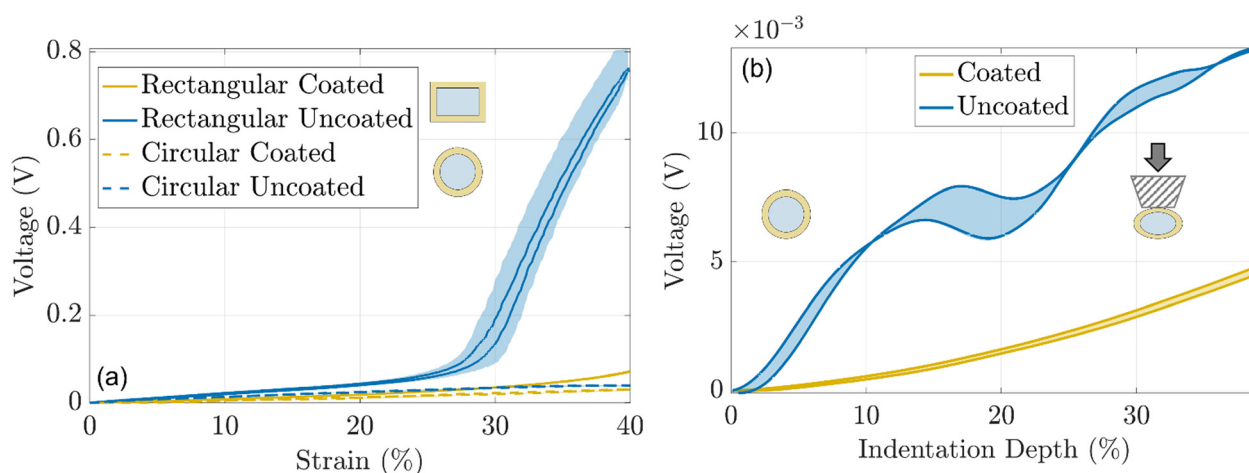

Fig. 6 (a) Variation of the voltage read by the photoreceiver during stretching of PDMS-based coated/uncoated rectangular waveguides and coated/uncoated circular waveguides. (b) Voltage at the photoreceiver *vs.* indentation depth of coated/uncoated circular PDMS waveguides. The filled portions of the curves represent the standard deviation.

showed the poorest performance upon stretching, the next characterizations were performed only on the circular ones.

The behavior of coated and uncoated circular waveguides upon indentation was investigated using *ad hoc* testing apparatus (5 cycles, 0.5 mm s^{-1}). The coated waveguide showed 3 fold lower optical losses compared to the uncoated one, for up to 40% of indentation depth (Fig. 6b). This result can be explained considering that for the uncoated waveguide, the indenter comes in contact with the core of the device and optical loss occurs due to frustrated total internal reflection (fTIR). For the waveguide with a reflective coating, the optical wave is internally reflected within the core with no significant loss since the indenter does not come in contact with the core material. Video S1 (ESI†) shows the performances of the uncoated and coated circular waveguides for arbitrary indentation profiles.

Moreover, the effectiveness of the TiO$_2$ coating for shielding environmental light was evaluated. The two waveguides were placed first in a black box and later under conventional laboratory conditions to measure the optical signal variance due to the presence of external light. The optical signal of the uncoated waveguide increased by about 22% witnessing that environmental light influenced the readout of the photoreceiver. Instead, the rise of the optical signal in the coated waveguide was only 0.6%, proving that the TiO$_2$ layer effectively shields the environmental light.

Finally, the two circular waveguides were qualitatively tested to evaluate their response by repeated manual deformation. Video S1 (ESI†) shows the different performances of coated and uncoated waveguides when they were indented, bent, and folded. The coated waveguide showed superior tolerance to indentation and bending showing an overall optical loss five times lower than the corresponding uncoated waveguide. This demonstrated the effectiveness of the TiO$_2$ coating in limiting the optical loss for different mechanical interactions by promoting internal light reflection.

Ecoflex10-base strain sensor. The operating principle of the optical sensor is described again by the Lamber–Beer law. However, in this case, the attenuation coefficient of Ecoflex-0010 is higher than that of PDMS (Fig. S5, ESI†), thus by elongating the device, *i.e.*, by increasing the optical path, a decrease in the transmitted light was expected. In Fig. 7a are reported 10 characterization cycles of the optical strain sensor elongated up to 110% at increasing strain rates (0.5 mm s^{-1}, 1 mm s^{-1}, and 5 mm s^{-1}). Upon stretching, the response of the photoreceiver increased following an exponential law before reaching saturation over 100% strain. Above this value, no voltage variation occurred as the light was fully absorbed by the core material. For all the tested strain rates, the characterization cycles were perfectly overlapped, proving the independence of the strain sensor from the strain rate (Fig. 7). However, at the highest strain rate, hysteresis between the
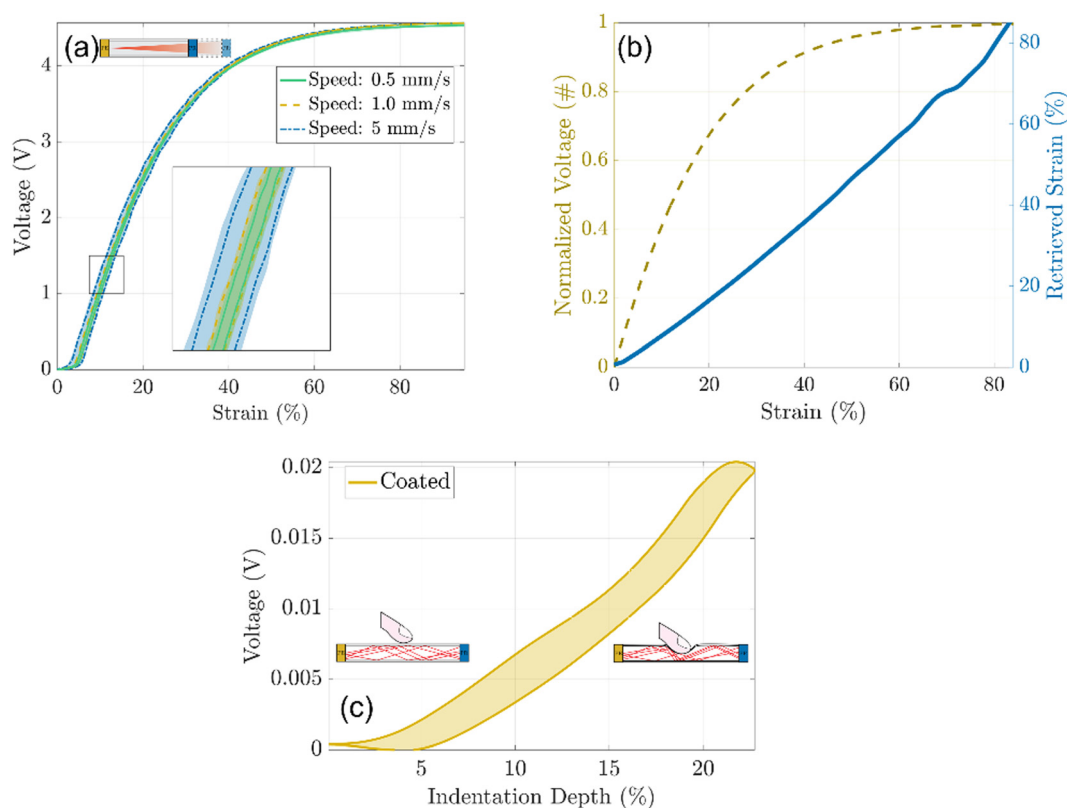

Fig. 7 (a) Voltage *vs.* strain% cycles of the optical strain sensor at increasing strain rate: 0.5, 1, and 5 mm s^{-1}. (b) Normalized and linearized characteristic curve of the optical strain sensor. (c) Variation in the voltage of the strain sensor when subjected to indentation. The filled portions of the curves represent the standard deviation of the measurements.

loading and unloading curves was observed within the 5–30% strain region probably due to the mechanical hysteresis of the sample itself. In order to linearize the characteristic curve of the sensor, the strain retrieved from the sensor was calculated as follows (eqn (3)):

$$\text{Retrieved strain (\%)} = -14.69 \times \ln(1 - V_{\text{norm}}) \quad (3)$$

where V_{norm} is the normalized voltage read at the photoreceiver (ranging between 0 and 1). The obtained curve had R_{sq} of 0.96 proving good fitting with a straight line with a slope equal to 1.

With this transformation, the characteristic curve showed a linear trend between 0 and 90% of the strain with sensitivity equal to 1/14.96 = 0.068, and an average resolution close to 1% which corresponds approximately to 100 μm.

As for the waveguides, the response of the optical strain sensor was evaluated upon indentation, bending, or folding (Video S2, ESI†). Owing to the reflective coating used as a cladding material, the optical sensor was slightly affected by the induced mechanical stresses. When the strain sensor was indented, the optical loss was two orders of magnitude lower than similar deformations at elongation (Fig. 7c). This proved the selectivity to a specific mechanical stimulus, as the developed optical sensor was mainly sensitive to stretching, while no important variations in the optical output were detected for compression or bending.

Finally, as the stretchable sensor is composed of a highly compliant material (Ecoflex-0010) it is expected to not physically burden the soft robot but easily follow its deformations.

The application of the reflective coating based on TiO_2 particles allowed to reflect internally the light when the device was bent or indented without any significant optical loss. As the reflective properties of the coating are only ascribable to the presence of titania particles, in principle, our approach can be easily implemented in other elastomeric matrices improving the performances of other soft optical devices.

Conclusions

In this work, a straightforward and inexpensive method to develop highly reflective coatings is proposed, for developing soft optical components (like waveguides also used as sensors), by adding TiO_2 particles in elastomeric matrices. Controlling the filler load and film thickness, the shielding abilities of the composite films are predicted for every wavelength belonging to the visible and near infra-red region of the electromagnetic spectrum. Moreover, the addition of the ceramic particles does not lead to stiffening of the material but rather to softening, making the developed coatings good candidates as cladding materials in stretchable waveguides and optical sensors. As a proof of concept, a PDMS-based waveguide and an Ecoflex-based optical sensor coated with the shielding coatings are demonstrated. They both show superior resistance to external mechanical stimuli such as bending, folding, and indentation, thanks to the internal reflection of light within the devices.

The possibility to produce stretchable optical sensors in a compliant material such as Ecoflex0010 is promising for soft robotics, since innovative sensorized skins could be developed in the near future without constraining the deformations of a soft robot. Finally, it is remarkable that as the reflective properties of the coatings are only linked to the presence of TiO_2 particles, it is possible to develop different elastomeric reflective composites, which can pave the way for new designs of optical sensors exploiting light reflection rather than their absorption.

Author contributions

S. L., M. L. P., and L. B. conceptualized research. S. L. and M. L. P. designed methodology, performed experiments, and analysed the data. S. L., M. L. and L. B. discussed the results and wrote the paper.

Conflicts of interest

There are no conflicts to declare.

Acknowledgements

Notes and references

1 L. Beccai, C. Lucarotti, M. Totaro and M. Taghavi, *Soft Robotics Mechanosensing*, ed. C. Laschi, J. Rossiter, F. Iida, M. Cianchetti and L. Margheri, Springer International Publishing, Cham, 2017, pp. 11–21.
2 J. Guo, C. Yang, Q. Dai and L. Kong, *Sensors*, 2019, **19**, 3771.
3 H. Wang, M. Totaro and L. Beccai, *Adv. Sci.*, 2018, **5**, 1800541.
4 M. Lo Preti, M. Totaro, E. Falotico and L. Beccai, *Electronic Skin: Sensors and Systems*, River Publishers, 2020, pp. 73–100.
5 D. Chen and Q. Pei, *Chem. Rev.*, 2017, **117**, 11239–11268.
6 H. Y. Tam, C.-F. J. Pun, G. Zhou, X. Cheng and M. L. V. Tse, *Opt. Fiber Technol.*, 2010, **16**, 357–366.
7 I. P. Johnson, W. Yuan, A. Stefani, K. Nielsen, H. K. Rasmussen, L. Khan, D. J. Webb, K. Kalli and O. Bang, *Electron. Lett.*, 2011, **47**, 271–272.
8 M. Umar, K. Min and S. Kim, *APL Photonics*, 2019, **4**, 120901.
9 Z. Liu, Z. F. Zhang, H.-Y. Tam and X. Tao, *Photonics*, Multi-disciplinary Digital Publishing Institute, 2019, vol. 6, p. 48.
10 C. Wu, X. Liu and Y. Ying, *ACS Sens.*, 2021, **6**, 1446–1460.
11 I. Martincek, D. Pudis and M. Chalupova, *IEEE Photonics Technol. Lett.*, 2014, **26**, 1446–1449.

12 J. Missinne, S. Kalathimekkad, B. Van Hoe, E. Bosman, J. Vanfleteren and G. Van Steenberge, *Opt. Express*, 2014, **22**, 4168–4179.

13 J. Guo, B. Zhou, C. Yang, Q. Dai and L. Kong, *Adv. Funct. Mater.*, 2019, **29**, 1902898.

14 C. K. Harnett, H. Zhao and R. F. Shepherd, *Adv. Mater. Technol.*, 2017, **2**, 1700087.

15 H. Zhao, K. O'Brien, S. Li and R. F. Shephered, *Sci. Robot.*, 2016, **1**, eaai7529.

16 J. A. Barreiros, A. Xu, S. Pugach, N. Iyengar, G. Troxell, A. Cornwell, S. Hong, B. Selman and R. F. Shephered, *Sci. Robot.*, 2022, **7**, eabi6745.

17 H. Bai, S. Li, J. Barreiros, T. Y. Tu, C. R. Pollock and R. F. Shephered, *Science*, 2020, **370**, 848–852.

18 A. Leber, B. Cholst, J. Sandt, N. Vogel and M. Kolle, *Adv. Funct. Mater.*, 2019, **29**, 1802629.

19 J. Guo, M. Niu and C. Yang, *Optica*, 2017, **4**, 1285–1288.

20 A. Heiden, D. Preninger, L. Lehner, M. Baumgarten, M. Drack, E. Woritzka, D. Schiller, R. Gerstmayr, F. Hartmann and M. Kaltenbrunner, *Sci. Robot.*, 2022, **7**, eabk2119.

21 V. Fang, J. V. Kennedy, J. Futter and J. Manning, *GNS Science Report*, 2013.

22 I. Roppolo, N. Shahzad, A. Sacco, E. Tresso and M. Sangermano, *Prog. Org. Coat.*, 2014, **77**, 458–462.

23 P. Jeevanandam, R. S. Mulukutla, M. Phillips, S. Chaudhuri, L. E. Erickson and K. J. Klabunde, *J. Phys. Chem. C*, 2007, **111**, 1912–1918.

24 J. Zhang, C. Zhu, J. Lv, W. Zhang and J. Feng, *ACS Appl. Mater. Interfaces*, 2018, **10**, 40219–40227.

25 S. Soumya, A. P. Mohamed, L. Paul, K. Mohan and S. Ananthakumar, *Sol. Energy Mater. Sol. Cells*, 2014, **125**, 102–112.

26 B. Xiang, X. Yin and J. Zhang, *Compos. Sci. Technol.*, 2017, **145**, 149–156.

27 L. Yuan, X. Weng, M. Zhou, Q. Zhang and L. Deng, *Nanoscale Res. Lett.*, 2017, **12**, 597.

28 F. H. Alkallas, K. M. Elshokrofy and S. A. Mansour, *Nanomater. Nanotechnol.*, 2019, **9**, 1–7.

29 H. Tang, H. Berger, P. E. Schmid and F. Lévy, *Solid State Commun.*, 1994, **92**, 267–271.

30 G. Riccucci, L. Pezzana, S. Lantean, A. Tori, S. Spriano and M. Sangermano, *Appl. Sci.*, 2021, **11**, 5663.

31 E. C. Murphy, J. H. Dumont, C. H. Park, G. Kestell, K.-S. Lee and A. Labouriau, *J. Appl. Polym. Sci.*, 2020, **137**, 48530.

32 J. González-Rivera, R. Iglio, G. Barillaro, C. Duce and M. R. Tinè, *Polymer*, 2018, **10**, 616.

33 G. Ouyang, K. Wang and X. Y. Chen, *J. Micromech. Microeng.*, 2012, **22**, 74002.

34 C. Markos, K. Vlachos and G. Kakarantzas, *Opt. Mater. Express*, 2012, **2**, 929–941.

35 D. K. Cai, A. Neyer, R. Kuckuk and H. M. Heise, *Opt. Mater.*, 2008, **30**, 1157–1161.

36 F. Schneider, J. Draheim, R. Kamberger and U. Wallrabe, *Sens. Actuators, A*, 2009, **151**, 95–99.

37 K. Hornik, M. Stinchcombe and H. White, *Neural Networks*, 1989, **2**, 359–366.

38 K. Hornik, *Neural Networks*, 1991, **4**, 251–257.

39 D. T. Vaimakis-Tsogkas, D. G. Bekas, T. Giannakopoulou, N. Todorova, A. S. Paipetis and N.-M. Barkoula, *Mater. Chem. Phys.*, 2019, **223**, 366–373.

40 M. Razzaghi Kashani, S. Javadi and N. Gharavi, *Smart Mater. Struct.*, 2010, **19**, 35019.

41 F. Carpi and D. D. Rossi, *IEEE Trans. Dielectr. Electr. Insul.*, 2005, **12**, 835–843.